Non-degenerate two photon absorption enhancement for laser dyes by precise lock-in detection

B. Xue, C. Katan, J. A. Bjorgaard, T Kobayashi

Non-degenerate two photon absorption enhancement for laser dyes by precise lock-in detection

B. Xue,[1,2] C. Katan,[3] J. A. Bjorgaard,[4,5] and T. Kobayashi[1,2,6,7,a]
[1]*Advanced Ultrafast Laser Research Center and Department of Engineering Science, Faculty of Informatics and Engineering, University of Electro-Communications, 1-5-1 Chofugaoka, Chofu, Tokyo, 182-8585, Japan*
[2]*Japan Science and Technology Agency, CREST, 5 Sanbancho, Chiyoda-ku, Tokyo, 102-0075, Japan*
[3]*Institut des Sciences Chimiques de Rennes, UMR 6226 CNRS-Université Rennes 1, 35042 Rennes, France*
[4]*Center for Nonlinear Studies, Los Alamos National Laboratory, Los Alamos, NM, United States*
[5]*Theoretical Division, Los Alamos National Laboratory, Los Alamos, NM, United States*
[6]*Department of Electrophysics, National Chiao-Tung University, Hsinchu, 30010, Taiwan*
[7]*Institute of Laser Engineering, Osaka University, 2-6 Yamada-oka, Suita, Osaka, 565-0871, Japan*

(Received 28 July 2015; accepted 21 December 2015; published online 31 December 2015)

This study demonstrates a measurement system for a non-degenerate two-photon absorption (NDTPA) spectrum. The NDTPA light sources are a white light super continuum beam (WLSC, 500~720 nm) and a fundamental beam (798 nm) from a Ti:Sapphire laser. A reliable broadband NDTPA spectrum is acquired in a single-shot detection procedure using a 128-channel lock-in amplifier. The NDTPA spectra for several common laser dyes are measured. Two photon absorption cross section enhancements are found in the experiment and validated by theoretical calculation for all of the chromophores. [http://dx.doi.org/10.1063/1.4939568]

I. INTRODUCTION

Interest in materials that exhibit high optical nonlinearity has increased dramatically in recent years. In particular, two-photon absorption (TPA) has been exploited in several current technologies, including optical power limiting,[1] all-optical shutter,[2] two-photon fluorescence microscopy,[3–5] and others.[6] Two-photon induced fluorescence (TPIF)[7–9] is the most frequently used method for measuring TPA spectra and cross sections in nonlinear materials, while the Z-scan method[10,11] is less commonly employed. However, to acquire broad information on TPA spectra, wide tunable laser sources such as an optical parametric amplifier or dye laser sources are needed.[7,12,13] But, even with a tunable source, the measurement must be repeated for each selected wavelength. As it is often impossible to maintain the experimental conditions throughout the time required to perform the measurement for each wavelength across the full spectral range, experimental errors are introduced. The instability in the peak intensity of the laser pulses also inevitably induces large experimental errors into this time-consuming measurement, a problem that is further enhanced by the nonlinearity of the process. Furthermore, due to the diversification in the pulse duration during the pulse wavelength shifting, the pulse intensity changes for each measurement. In addition, these methods are indirect ways to measure the TPA spectrum, and thus may suffer from other systematic errors related to the intermediate parameters, such as the collection efficiency of emitted fluorescence, fluorescence quantum efficiency, and so on.[7] Finally, the degenerate detection's intensity squared dependence on the excitation beam intensity may lead to a large error during the square calculation. Such inaccuracies may affect the measurements

[a]Corresponding author: kobayashi@ils.uec.ac.jp

and may explain the quite different TPA cross section values that have been reported when the same method is used to examine some well-known materials.[5,7,12,14,15]

In 1999, Belfield *et al*. reported for the first time an method for measuring the non-degenerate TPA (NDTPA) spectrum using a pump-probe two-beam configuration[16] in which the strong pump was a monochromic IR laser beam and the weak probe was a white-light super-continuum (WLSC) beam. In this setup, a broad TPA spectrum can be directly measured in a single procedure by the spectral subtraction of the absorbed probe beam from the reference beam. The pump beam intensity has a linear dependence on the TPA cross section (as discussed later), which apparently induces a lower level of error than the intensity squared degenerate detection. However, the acquired spectrum difference is time dependent due to the overlapping time shift between pump and probe beams. This is due to the chirping effect occurring during the WLSC generation and the group-velocity dispersion (GVD) effect on the probe pulse propagation time. Kovalenko *et al*. proved that the chirp could be eliminated by using time-correction procedure when using a supercontinuum probe.[17] However, since the publication of the work by Belfield *et al*., there have only been a few reports using this setup for a limited number of direct-gap semiconductors and semiconductor quantum dots.[18,19]

In this study, we improve this method in several ways. First, we use chirp mirror pairs to compress the WLSC pulses before propagation in the sample. A very broad WLSC is generated via complex processes that include a self-phase modulation, plasma generation, and stimulated Raman scattering. Due to the different contributions of these phenomena to the generation mechanism, the transient refractive index change is wavelength dependent in a very complicated way. Therefore, it is difficult to compress the chirp of WLSC. To minimize the chirp effect in our detector, we replace the spectrometer used in Belfield's setup with a time-resolved two-dimensional induced absorption (ΔA) spectrum map obtained by combining a polychromater with a multi-channel lock-in amplifier (MLA).[16] This ΔA map is of vital importance for determining the pump and probe pulse overlapping position in time. The MLA not only causes a large improvement of the signal noise ratio (SNR), but also makes it possible to simultaneously and directly measure a broadband difference absorption spectrum with 128 spectral points and a spectral resolution of 0.83 nm. With this high performance equipment, the TPA profiles for several laser dyes. The TPA spectra thus obtained are confronted to theoretical predictions to further validate our approach.

II. THEORY

In general, the attenuation of a light beam passing through an optical medium along an axis, designated here as the z-axis, can be expressed by the following phenomenological expression (this case includes linear and nonlinear interactions):[20]

$$\frac{dI(z)}{dz} = -\alpha I(z) - \beta I^2(z) - \gamma I^3(z) - \cdots. \tag{1}$$

Here, I(z) is the intensity of the incident light beam propagating along the z-axis and α, β, and γ are the one-, two-, and three-photon absorption coefficients of the transmitting medium, respectively. To compare the absorption induced by the two-photon process in the case of an incident laser with a negligible bandwidth to the electronic bandwidths relevant to the two-photon transition including virtual states, we have the following:

$$\frac{dI(z)}{dz} = -\beta I^2. \tag{2}$$

The non-degenerate condition, in our situation for an intensity I_1 of the WLSC probe beam and I_2 for the pump beam, leads to:

$$\frac{dI_1(z)}{dz} = -\beta_1 I_1 I_2. \tag{3}$$

$$\frac{dI_2(z)}{dz} = -\beta_2 I_1 I_2. \tag{4}$$

Here, the two-photon absorption coefficient β is linear and proportional to the imaginary part of the third order nonlinear susceptibility as given by[21]

$$\beta_{1,2} = \frac{8\pi^2\omega_{1,2}}{c^2\varepsilon_1^{1/2}\varepsilon_2^{1/2}}\mathrm{Im}\chi(-\omega_1;\omega_1,-\omega_2,\omega_2). \quad (5)$$

ε_i denotes the dielectric constant at the angular frequency of ω_i for each incident light, and c is the velocity of light. For input (before the medium) beam intensities labeled I_{10} and I_{20}, and considering the case where $I_{20} >> I_{10}$, Eqs. (3) and (4) can be solved as follows

$$I_2 \cong I_{20}. \quad (6)$$

$$I_1 \cong e^{-\beta_1 I_{20} z} I_{10} \quad . \quad (7)$$

Then,

$$\beta_1 I_{20} z = -\ln\frac{I_1}{I_{10}} = -\frac{1}{\lg e}\lg\frac{I_1}{I_{10}} = \frac{1}{\lg e}\Delta A \quad . \quad (8)$$

This condition is met in our setup as the intensities at the sample position of the pump and the probe within the spectral resolution are estimated to be 15 GW/cm^2 and 0.1 GW/cm^2, respectively. From Eq. (8), it is easy to see that with an intense pump, the TPA coefficient is linear in proportion to the pump beam-induced WLSC probe beam absorbance difference (ΔA). The relationship between the TPA cross section σ in cm^4/GW) and TPA coefficient (in cm/GW) is given by[17]

$$\beta_1 = \sigma N_A c \times 10^{-3}, \quad (9)$$

where N_A is the Avogadro constant and c is the concentration of the sample (in M). From Eqs. (8) and (9), we can conclude that the TPA cross section is proportional to the absorbance change ($\sigma \propto \Delta A$). As ΔA can be directly acquired through the pump probe experiment, the TPA cross section can be calculated from experimental data without interference from other error sources (vide supra). Noteworthy, in this study, all spectra reporting TPA cross sections are based on the transformed TPA wavelength, which is the relative value calculated using ($2/\lambda_{TPA} = 1/\lambda_{pump} + 1/\lambda_{probe}$).

III. EXPERIMENTAL PROCEDURES

We use a pulse energy of about 200 μJ from the Spitfire Ace Laser system (Spectra Physics, 1 kHz repetition rate, central wavelength at 798 nm). Total energy is divided into two using a 10% reflection beam splitter. The transmitted beam affords the pump beam, while the reflected beam is used to generate the WLSC, focusing the fundamental beam on a 2-mm-thick sapphire plate. The strong fundamental part of the beam is blocked by transmitting the beam through a 720 nm short pass dichroic mirror. The WLSC spectral range is from 500 nm to 730 nm. A pair of chirp mirrors (GVD, 470~810 nm, -40 ± 20 fs^2) are used to slightly compress the WLSC beam with a triple-pass configuration. Next, the WLSC probe beam and the time-delayed pump beam are both focused using an off-axis parabolic mirror and overlapped at the sample point. After passing through the sample, the beams are collimated by another off-axis parabolic mirror. The pulse duration of the fundamental pump beam is measured as 103 fs using the SHG-FROG method.[22] The spot size of the focused pump beam at the sample surface is measured with a CCD beam profiler (Thorlabs) that has x- and y-axis of 146.1 and 149.9 μm, respectively. For data collection, the WLSC probe beam is focused into a multimode fiber, which is guided to the polychrometer, where the signal is captured by a 128-channel MLA. A synchronized chopper with half of the laser repetition frequency is introduced into the fundamental beam path and provides the reference frequency signal for the MLA. The pump beam power is controlled by a wheel gradient-neutral density filter set in the pump path.

Several types of organic fluorescent dyes are used as target samples in this study. They are two xanthene dyes, rhodamine 6G and rhodamine 123 ([6-amino-9-(2-methoxycarbonylphenyl)xanthen-3-ylidene]azanium chloride), dissolved in methanol; two coumarins dyes, coumarin 6 (3-(2-Benzothiazolyl)-7-diethylamino-coumarin) and coumarin 343 (2,3,6,7-Tetrahydro-11-oxo-1H,5H,11H-[1]benzopyrano[6,7,8-ij]quinolizine-10-carboxylic acid), dissolved in chloroform; and two oxazine dyes, Nile red (9-diethylamino-5-benzo[α]phenoxazinone) and Nile blue A (Basic blue 12), dissolved in chloroform. All of the dyes are purchased from Sigma-Aldrich and used without further purification.

IV. RESULTS AND DISCUSSION

A typical result for our TPA spectrum measurement procedure is shown in Fig. 1. The sample is coumarin 6 dissolved in chloroform at a concentration of 23.7 mM. The time-resolved two-dimensional difference absorbance (ΔA) spectra of the probe beam (WLSC) is shown in Fig. 1(a). The large positive signal located at the center, around 560 nm, with a delay time of around zero, corresponds to the TPA effect. The black solid line traces the peak of this ΔA map; it shows the zero time position where the pump and probe pulses overlap.[17] The twists in this peak-tracing line are due to residual chirp of the WLSC and its group velocity dispersion (GVD) in the solvent. The TPA cross section spectrum of coumarin 6 is shown in Fig. 1(b). It has a spectral resolution of about 10 nm, which is due to the FWHM of pump spectral shape. For coumarin 6, the results shows a TPA peak located at 652 nm with a cross section of 1015 ± 107 GM. This TPA band is in fairly good agreement with the computed NDTPA spectra (Fig. S2), given the different approximations that cannot be avoided (see Supplemental Material[30] for details).

The two-dimensional ΔA map for rhodamine 6G dissolved in methanol (concentration: 16.2 mM) is shown in Fig. 2(a). Due to losses caused by the stationary absorption of the sample solution, the WLSC probe spectral range is limited to the lowest end at 562 nm. A large positive ΔA signal is observed for the probe wavelength range from 562 nm to 658 nm. Noticeably, in the same spectral range, some large negative signals appear with delay times longer than 100 fs, and the intensity decreases as the wavelength increases. The comparison of this pattern with its spontaneous fluorescence spectrum, confirms that it is the result of the stimulated emission (SE) of rhodamine 6G. This SE can also be observed in the ΔA map of coumarin 6 when the intensity scale is narrowed, although the intensity is too weak to be perceived directly in Fig. 1(a).

The TPA is one of the most common third-order nonlinear optical processes, but other third-order nonlinear effects, such as stimulated Raman scattering, have already been well-studied using a similar non-degenerate pump-probe setup.[17] In this work, we stress that a strong stimulated Raman loss[23] (SRL) signal is found in a blank test made of methanol solvent. The details are shown in Fig. 2(b). An inverted triangle shaped signal is located near 645 nm; its intensity distribution has a two peak structure. These two peaks are caused by the Raman shift of 3000 cm^{-1} and 3300 cm^{-1}, respectively, which correspond to the -CH_3 asymmetric stretch and the -OH stretch. Many common solvents, such as ethanol, DMSO, water and so on, have similar intense SRL signals in this spectral range. These additional signals must be rigorously accounted for in dye measurements. Carbon tetrachloride (CCl_4) or chloroform ($CHCl_3$) are the recommended solvents for experimental verification as they do not have a large SRL signal around 3000 cm^{-1}. Unfortunately, many common dyes such as xanthene dyes do not readily dissolve in such solvents. Therefore, solvents with intense Raman signals in the probe spectral range must sometimes be used, and it is necessary to account for the contribution a Raman solvent makes to the observed TPA spectrum. The comparison of Fig. 2(a) with Fig. 2(b) shows that the TPA signal of the sample is contaminated with a Raman loss signal induced in the solvent; the contamination range is marked with a circle of red dots.

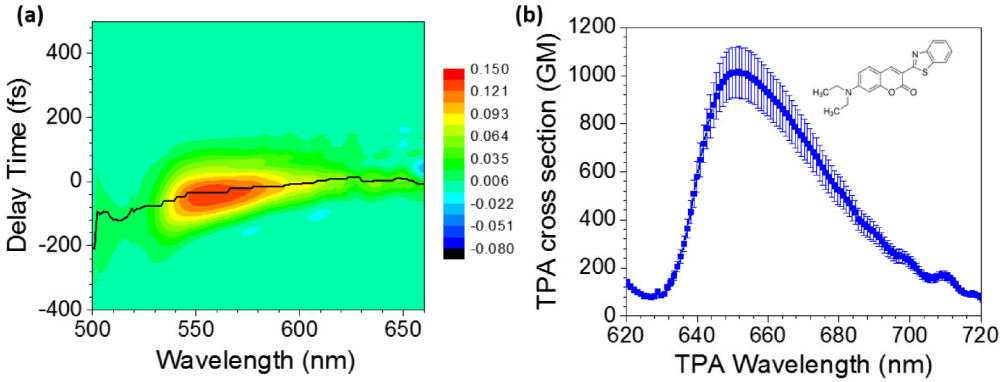

FIG. 1. (a) Two-dimensional absorbance change of WLSC through coumarin 6 dissolved in chloroform. (b) TPA cross section spectrum of coumarin 6 in chloroform.

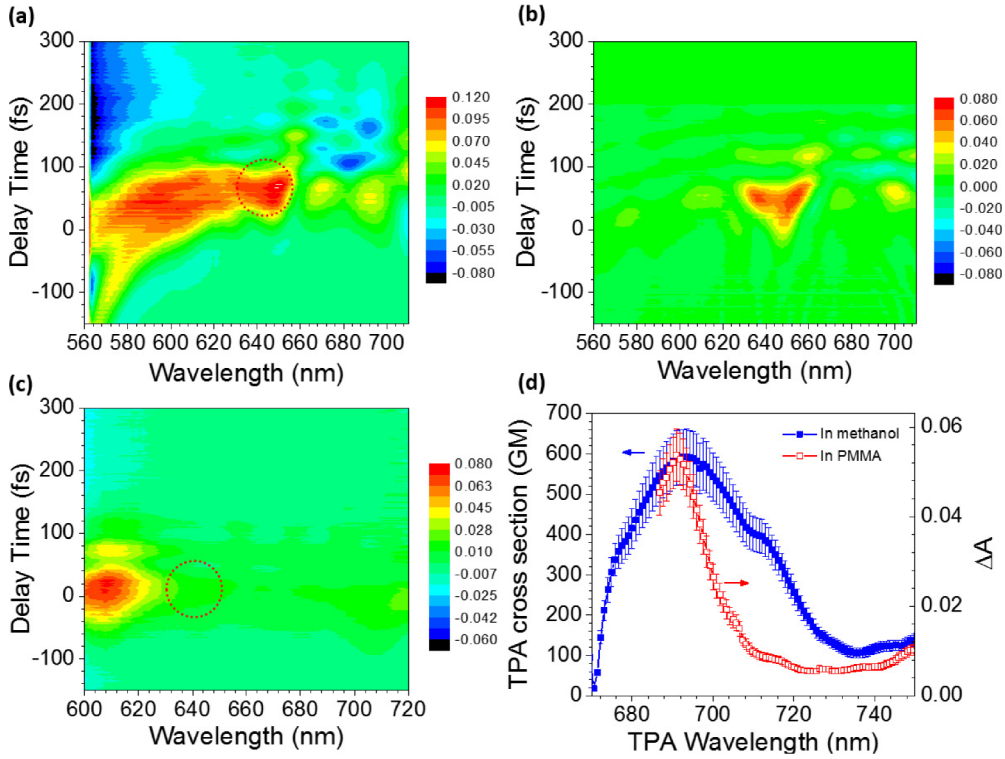

FIG. 2. (a) Two-dimensional absorbance change of WLSC through rhodamine 6G dissolved in methanol. (b) Background test for solvent methanol only. (c) Absorbance change of WLSC through rhodamine 6G doped in PMMA film. (d) Measured TPA cross section spectrum of rhodamine 6G in methanol and PMMA.

It is difficult to distinguish the SRL's contribution to the TPA signal when they are spectrally overlapping, as they are both two-photon processes belonging to the comparable third-order nonlinear effects.[17,22] The two incident beams (WLSC (ω_1) and 800 nm (ω_2)) can interact with each other in time overlapping conditions, and both the ω_1 photons and the ω_2 photons can be absorbed during a TPA process. In the same way, when associated with the ω_1 photons, the ω_2 photons can be absorbed (scattered) by the Stokes mechanism or can be amplified by the anti-Stokes mechanism if the vibrational difference level corresponding to the frequency difference ($\omega_1 - \omega_2$) is populated. The latter case is not fulfilled in this experiment. Furthermore, coupling between the TPA and Raman processes may occur if the solvent levels in the sample (including at the solvent molecule level) are coherently coupled.

The vibronic states of solvent molecules do not lead to strong coupling with the solute vibronic states due to the lack of strong interaction through the hydrogen bonding. Therefore, there is no "intrinsic" interference between the electronic polarization and the solute molecule coherence in the solvent system. However, an extrinsic interference is possible. For example, interference may occur if an amplified ω_2 photon created via a stimulated Raman scattering by ω_1 photons is used in the TPA together with ω_1. The Raman gain expected for a ω_2 photon when ω_1 photons exist can be estimated by the Raman correspondence of the solute molecule with a 24.7 M concentration. It is 5×10^{12} photons/cm^{2}sec when the number of ω_1 photons is 2×10^{16} photons/cm^{2}sec. The loss of the probe light through this process can be completely negligible, and the following equation can be used:

$$\Delta A(\omega) = \Delta A_{TPA}(\omega) + \Delta A_{RS}(\omega). \tag{10}$$

Here, ΔA_{TPA} and ΔA_{RS} refer to the TPA and Raman effect, respectively. For the solvent sample, which is a mixture of the solute and solvent, the effect of both should be considered. Especially in this setup, it is expected that the TPA will not create interference, even in the neat solvents, as the absorption edge of the solvent molecules are located much higher (blue side) than the half of the

shortest edge of the continuum spectrum. However, Raman scattering of the solute scarcely occurs in a relative Raman shift larger than 2000 cm^{-1}. Even if, due to the solute in the sample, the Raman signal makes a contribution, it is expected to have a negligibly low intensity as the concentration of the dyes molecules is lower than the concentration of solvent molecules by the factor of 10^{-3}. The concentrations of the solute and solvent in the experiment are calculated to be 24.7 M and 8.1×10^{-3} M, respectively. Therefore, from the right part of the Eq. (10), it can be concluded that ΔA_{TPA} is a measure of the solute only, and ΔA_{RS} is a measure of the solvent only.

A polymethyl methacrylate (PMMA) thin film doped with rhodamine 6G is investigated with the expectation of directly removing the solvent interference. PMMA has a large molecular weight and is transparent in the visible and near IR light range; thus, it is expected to be an appropriate matrix to investigate TPA of organic molecules. The PMMA powder and rhodamine 6G are both dissolved in chloroform and mixed with each other; then the mixture is dried and spin-coated on a glass plate. After being stripped from the slide, the film is used for the measurement. The measured ΔA map in Fig. 2(c) shows that this sample does not have a large ΔA peak around 645 nm (red dash circle mark), which means the Raman background effect is efficiently minimized. However, it is difficult to directly determine the TPA cross section with this doped PMMA film, because it is difficult to precisely determine the film thickness and the number of dissolved molecules, as the molecules in the polymer matrix sample are inhomogeneous. This is a serious problem in any kind of spectroscopic measurement of doped molecules in a polymer film. In spite of this, the relative values of the TPA cross section recorded at different wavelengths are reliable due to the broadband measurement. This is verified with several scans. Fig. 2(b) suggests that, for the probe range 580 nm to 600 nm, the distortion effect from the solvent is negligible. Then, by assuming that rhodamine 6G has the same TPA properties in methanol as in PMMA, we can reconstruct a more reliable TPA cross section spectrum by merging and scaling the result in PMMA to the methanol case. Fig. 2(d) shows that the measurement starts with the blue round line from 670 nm and transforms into the red open square line around 690 nm. The optimized TPA peak is located at 691 nm with a cross section of 596 ± 69 GM. This result is discussed in more detail in the next section.

We use a sample of rhodamine 6G in methanol to study the dependence of the TPA cross section on the pump power and sample concentration. To examine pump power dependence, the sample is fixed at a concentration of 16.2 mM. The pump power is adjusted to between 40 μW and 840 μW with a neutral density filter. For convenience, we track the ΔA peak values at 620 nm probe wavelength on each ΔA map acquired by different pump power; they are shown as blue triangle marks in Fig. 3. The linear fitting has a nearly zero intercept, which shows a good agreement with Eq. (8).

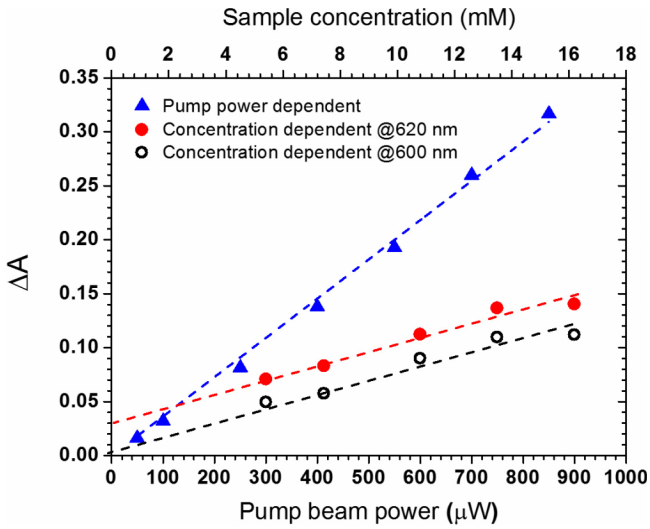

FIG. 3. Pump power dependence (blue triangle) and sample concentration dependence (red round and black circle) in rhodamine 6G TPA cross section measurement.

As shown in Fig. 3, there is almost no visible saturation of TPA in this pump power range. For the concentration dependence measurement, the pump power is fixed at 400 μW. Several samples with different concentrations are investigated in a similar way: ΔA peak values at 600 nm and 620 nm for each concentration are marked with black circles and red round lines in Fig. 3, respectively. The linear fitting for each group shows that the 600 nm ΔA data has a nearly zero intercept, while the 620 nm clearly does not. This non-zero intercept evidences the above mentioned solvent's SRL interference, while zero intercept fitting lines are examples of a purely TPA phenomenon.

Having clarified all these issue, we can further investigate other dyes: rhodamine 123 (4.2 mM) dissolved in methanol and coumarin 343 (27.3 mM), Nile red (0.75 mM), and Nile blue A (0.68 mM) dissolved in chloroform. The choice for chloroform, despite its low solubility for the chosen solutes, is based on minimum SRL contribution to avoid contamination of the TPA signal. Corresponding TPA cross sections are shown in Fig. 4 (black square dotted line). The rhodamine 6G, rhodamine 123, coumarin 6, coumarin 343, Nile red and Nile blue A show efficient TPA peaks at 691 nm, 660 nm, 652 nm, 651 nm, 669 nm and 626 nm, respectively. The corresponded NDTPA cross sections are 596 GM, 776 GM, 1015 GM, 49 GM, 3270 GM and 1407 GM, respectively.

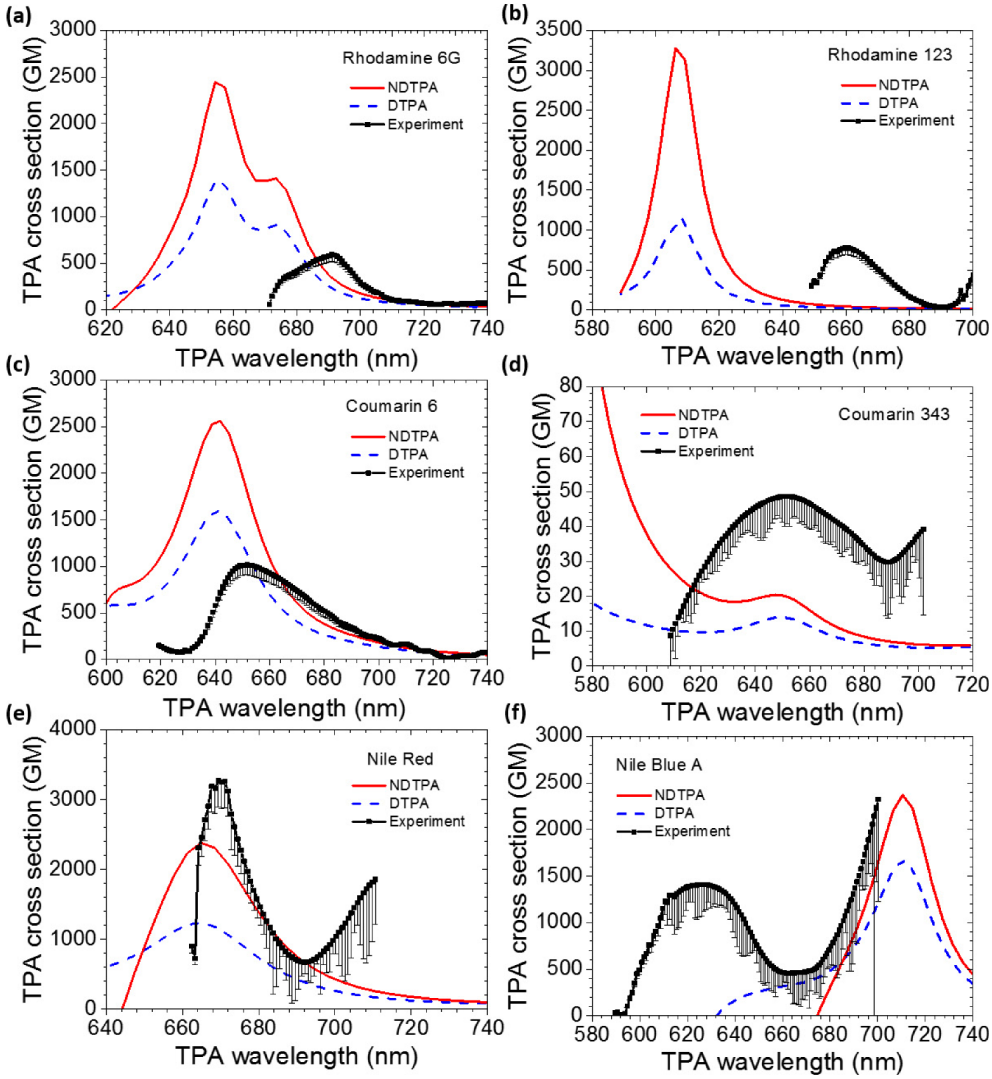

FIG. 4. Measured and calculated TPA cross section for (a) rhodamine 6G, (b) rhodamine 123, (c) coumarin, 6 (d) coumarin 343 (e) Nile red and (f) Nile blue A. In each figure, black solid line with error bar are the measured experimental value; calculated DTPA and NDTPA spectrum (800 nm pump) are plotted in blue dash line and red solid line.

TABLE I. Measured rhodamine 6G TPA cross section value compared with previous literature.

Reference	Wavelength (nm)	TPA cross section (GM)	Method	Laser	Pulse duration
14	694	180 ± 20	NLT[a]	Ruby	15 ps
15	694	355 ± 170	TPIF[b]	Ruby	40 ns
7	690 700 720	120 150 38	TPIF	Ti:Sapphire	100 fs
12	680 694 710	55 112 ± 12 94	TPIF	OPA	160 fs
This work (include errors)	675.7 683.4 691.0 699.3 707.4	337 ± 40 486 ± 57 596 ± 69 324 ± 36 139 ± 15	NWLP[c]	WLSC	103 fs[d]

[a]NLT: nonlinear transmission.
[b]TPIF: two photon induced fluorescence.
[c]NWLP: nondegenerate white light probe.
[d]Pump pulse duration.

In general, all of the results in this study evidence a larger TPA peak value than those reported using degenerate conditions. In fact, Table I compares the rhodamine 6G TPA cross sections obtained in this work to previously published values performed using degenerate conditions. The results all agree that the position of the TPA peak is around 690 nm. Obviously, our NDTPA values are larger than the DTPA found in other reports. Noteworthy, ns pulses are known to overestimate TPA cross sections, especially due to excited state absorption (the two-photon absorption can be non simultaneous). Some studies have reported that the NDTPA is usually enhanced as compared to DTPA.[20,25] This phenomenon can be explained as an intermediate state resonance enhancement (ISRE); one of the photons can have an energy close to one of the molecular excitation energies, and will achieve intermediate state resonance.

To get theoretical confirmation of our experimental results, we have implemented quantum chemical and few states approaches for both linear and nonlinear optical responses of the chromophores of interest. We use density functional theory (DFT) and time-dependent (TD) DFT approaches, as implemented in the Gaussian 03 and 09 packages.[26,27] No simplifications are made for the chemical structures. The properties of interest are related to ground state geometry: that is, geometry optimization and one- and two-photon absorption is related to the electronically excited states (ES). The polarizable continuum model (PCM) as implemented in Gaussian 09 and Gaussian 03 is used to simulate the solvent effects on geometries and optical spectra, respectively. No additional local field corrections are considered.[28] Optical spectra are obtained using the density matrix formalism for non-linear optical responses as proposed by Tretiak and Chernyak.[28,29] Absolute TPA amplitudes are derived using expression (38) of Ref. 28 for degenerate two-photon absorption (DTPA) considering both diagonal and non-diagonal contributions. For non-degenerate TPA, the TPA cross section is related to the imaginary part of the third-order polarizability $\gamma(-\omega_1;\omega_1,-\omega_2,\omega_2)$ and the frequency dependent prefactor ω^2 is replaced by $2{\omega_1}^2\omega_2/(\omega_1+\omega_2)$ as in Ref. 24, where index 1 refers to the probe beam and index 2 refers to the pump beam. The calculated TPA spectra shown in Fig. 4 are obtained at the TD-B3LYP/6-311+G*//B3LYP/6-311+G* level of theory in conventional quantum chemical notation "single point//optimization level" including up to 20 singlet ES. Given the overall good agreement between the experimental and theoretical OPA band positions (Fig. S1), NDTPA spectra were computed for the experimental pump wavelength only (1.55 eV/800nm).The

damping factor introduced to simulate the finite line width Γ in the resonant spectra is fixed according to Table S1 in the Supplemental Material.[30] The ES structure was further checked at the TD-ω B97xD/6-311+G*//B3LYP/6-311+G* level. More details for the calculation are included in the Supplemental Material.[30]

The calculated TPA cross sections are significantly larger than the experimental results shown in Fig. 4. This may be attributed to a number of factors related to the level of theory in use. First, B3LYP, the most suitable exchange-correlation functional in Gaussian 03 for optical properties, is known to overestimate conjugation and thus reduce bond length alternation and overestimate transition dipole moments.[31] For example, if the TPA cross section scales as the fourth power of dipole moment matrix elements (see expressions S1-S3 in the Supplemental Material[30]), a 15% overestimation of the dipole moments may double the TPA cross section. Next, the choice for the finite line width, which is set the same for all ES, directly affects the TPA amplitudes. In fact, when the two-photon excited state is near resonance, the TPA amplitude scales as 1/Γ (Fig. S2). In addition to local field corrections such as dynamic contributions,[28] other contributing factors include all of those currently considered in predictions of linear optical properties (band shape, amplitude and position) of solvated chromophores.[32] Specifically, the present solvation model is limited and does not account for state specific responses,[33] or for explicit solvent molecules or counter-ions. Furthermore, vibronic contributions[34] are not simulated. Despite all of these approximations, this level of theory has already proved efficient for rationalizing experimental TPA spectra.[28,33] The OPA spectra are systematically blue shifted compared to the experimental results. However, compared to the TD-B3LYP/6-31G(d)//HF/6-31G(d) level of theory in a vacuum, both the solvent and a larger basis set improve the agreement between calculated and experimental results. Given the small spectral window investigated experimentally, to be compared with the error in the calculated peak position (vide supra), these TPA spectra reveal a TPA band that is close to that experimentally observed. These bands, which have significant magnitude, are related to one (or several) higher lying excited state(s). Comparison between DTPA and NDTPA calculated spectra (Fig. 4) clearly demonstrate the intermediate state resonance enhancement experimentally observed. , which depends on the excited state structure of the particular chromophore. In fact, further intuitive understanding may be gained from few states models as discussed in details in the supplementary information. Besides the larger ISRE for rhodamines as compared to coumarins, the various transition energies taken for the TPA states for Nile Red and Nile blue A (Table S2) evidence the strong influence of respective transition energies compared to pump and probe photon energies on the overall enhancement factor.

V. CONCLUSION

In this study, we improve the method for measuring non-degenerate TPA cross sections by introducing an MLA system into the detection setup. With this system, high resolution and precise chirping correction is achieved using a ΔA map. However, this method still requires further improvement. First, many solvents, such as water and methanol, contribute a strong Raman loss signal with a Raman shift around 3000 cm^{-1} ~ 3300 cm^{-1}. This disturbance can be minimized by selecting an appropriate solvent and by properly correcting for the Raman effect. Second, the TPA spectrum detection range is limited to between 600 and 760 nm, when using 800 nm pumps, as in this study. This problem can be solved by choosing a solvent like chloroform or by changing the pump beam wavelength to a variable range with an OPA setup. Another feasible and easily available solution is to use a much wider WLSC, such as one generated by tapped fiber or photon crystal fiber.[35]

This study measures the TPA spectrum for several types of the laser dyes including xanthene dyes (rhodamine 6G and rhodamine 123), coumarin dyes (coumarin 6 and coumarin 343), and oxazine dyes (Nile red and Nile blue A). By comparing the results for our analysis of rhodamine 6G to published degenerate measurements, we confirm that TPA is enhanced in non-degenerate cases. We verify this conclusion with theoretical calculations. To the best of our knowledge, this is the first report of measurements for the other laser dyes sampled here. This method makes the measurement of TPA spectrum of materials much more convenient. It contributes to the new TPA materials development, and has already been applied by our collaborators.[36]

ACKNOWLEDGMENTS

This work is supported by the National Science Council of the Republic of China, Taiwan (NSC 98-2112-M-009-001-MY3), and a grant from the Ministry of Education, Aiming for Top University (MOE ATU) Program at National Chiao-Tung University (NCTU). This study is financially supported by a Grant-in-Aid for Scientific Research (No. 24740261) received from the Japan Society for the Promotion of Science and a joint research project at the Institute of Laser Engineering, Osaka University, under contract number B1-27. The research has been also supported by "100 Talents Program of The Chinese Academy of Sciences". C.K. acknowledges the HPC resources of CINES and of IDRIS under the allocations 2014-[x2014080649] and 2015-[x2015080649] made by GENCI (Grand Equipement National de Calcul Intensif). JAB acknowledges support of the U.S. Department of Energy through the Los Alamos National Laboratory (LANL) LDRD Program. LANL is operated by Los Alamos National Security, LLC, for the National Nuclear Security Administration of the U.S. Department of Energy under contract DE-AC52-06NA25396. We also acknowledge support of the Center for Nonlinear Studies (CNLS) at LANL and Sergei Tretiak for helpful discussion.

[1] G.S. He, J.D. Bhawalkar, C.F. Zhao, and P.N. Prasad, Appl. Phys. Lett. **67**, 2433 (1995).
[2] M.A.M. Versteegh and J.I. Dijkhuis, Opt. Lett. **36**, 2776 (2011).
[3] W.R. Zipfel, R.M. Williams, and W.W. Webb, Nat Biotech **21**, 1369 (2003).
[4] W. Denk, Proc. Natl. Acad. Sci. USA **91**, 6629 (1994).
[5] S.W. Hell, M. Booth, S. Wilms, C.M. Schnetter, A.K. Kirsch, D.J. Arndt-Jovin, and T.M. Jovin, Opt. Lett. **23**, 1238 (1998).
[6] A. Hayat, A. Nevet, P. Ginzburg, and M. Orenstein, Semicond. Sci. Tech. **26**, 083001 (2011).
[7] C. Xu and W.W. Webb, J. Opt. Soc. Am. B **13**, 481 (1996).
[8] M. A. Albota, C. Xu, and W.W. Webb, Appl. Opt. **37**, 7352 (1998).
[9] Y. Tan, Q. Zhang, J. Yu, X. Zhao, Y. Tian, Y. Cui, X. Hao, Y. Yang, and G. Qian, Dyes and Pigments **97**, 58 (2013).
[10] A. Nag, A. K. De, and D. Goswami, J. Phys. B: At. Mol. Opt. Phys. **42**, 065103 (2009).
[11] Y. Xia, Y. Jiang, R. Fan, Z. Dong, W. Zhao, D. Chen, and G. Umesh, Opt. Laser Technol. **41**, 700 (2009).
[12] N.S. Makarov, M. Drobizhev, and A. Rebane, Opt. Express **16**, 4029 (2008).
[13] M. Drobizhev, S. Tillo, N.S. Makarov, T.E. Hughes, and A. Rebane, J. Phys. Chem. B **113**, 855 (2009).
[14] P. Sperber and A. Penzkofer, Opt. Quant. Electron. **18**, 381 (1986).
[15] J.P. Hermann and J. Ducuing, Opt. Commun. **6**, 101 (1972).
[16] K.D. Belfield, D.J. Hagan, E.W. Van Stryland, K.J. Schafer, and R.A. Negres, Org. Lett. **1**, 1575 (1999).
[17] S.A Kovalenko, A.L. Dobryakov, J. Ruthmann, and N.P. Ernsting, Phys. Rev. A **59**, 2369-2383 (1999).
[18] C.M. Cirloganu, L.A. Padilha, D.A. Fishman, S. Webster, D.J. Hagan, and E.W. Van Stryland, Opt. Express **19**, 22951 (2011).
[19] L.A. Padilha, J. Fu, D.J. Hagan, E.W. Van Stryland, C.L. Cesar, L.C. Barbosa, C.H.B. Cruz, D. Buso, and A. Martucci, Phys. Rev. B **75**, 075325 (2007).
[20] G.S. He, L.-S. Tan, Q. Zheng, and P.N. Prasad, Chem. Rev. **108**, 1245 (2008).
[21] Y.R. Shen, *The Principles of Nonlinear Optics* (J. Wiley, New York, 1984), p. 203.
[22] K.W. DeLong, R. Trebino, J. Hunter, and W.E. White, J. Opt. Soc. Am. B **11**, 2206 (1994).
[23] B. Mallick, A. Lakhsmanna, and S. Umapathy, J. Raman Spectrosc. **42**, 1883 (2011).
[24] J.M. Hales, D.J. Hagan, E.W. Van Stryland, K.J. Schafer, A.R. Morales, K.D. Belfield, P. Pacher, O. Kwon, E. Zojer, and J.L. Bredas, J. Chem. Phys **121**, 3152 (2004).
[25] E. Roussakis, J.A. Spencer, C.P. Lin, and S.A. Vinogradov, Anal. Chem. **86**, 5937 (2014).
[26] Gaussian 03, Revision D.02, M.J. Frisch, G.W. Trucks, H.B. Schlegel, G.E. Scuseria, M.A. Robb, J.R. Cheeseman, J.A. Montgomery, Jr., T. Vreven, K.N. Kudin, J.C. Burant, J.M. Millam, S.S. Iyengar, J. Tomasi, V. Barone, B. Mennucci, M. Cossi, G. Scalmani, N. Rega, G.A. Petersson, H. Nakatsuji, M. Hada, M. Ehara, K. Toyota, R. Fukuda, J. Hasegawa, M. Ishida, T. Nakajima, Y. Honda, O. Kitao, H. Nakai, M. Klene, X. Li, J.E. Knox, H.P. Hratchian, J.B. Cross, V. Bakken, C. Adamo, J. Jaramillo, R. Gomperts, R.E. Stratmann, O. Yazyev, A.J. Austin, R. Cammi, C. Pomelli, J.W. Ochterski, P.Y. Ayala, K. Morokuma, G.A. Voth, P. Salvador, J.J. Dannenberg, V.G. Zakrzewski, S. Dapprich, A.D. Daniels, M.C. Strain, O. Farkas, D.K. Malick, A.D. Rabuck, K. Raghavachari, J.B. Foresman, J.V. Ortiz, Q. Cui, A.G. Baboul, S. Clifford, J. Cioslowski, B.B. Stefanov, G. Liu, A. Liashenko, P. Piskorz, I. Komaromi, R.L. Martin, D.J. Fox, T. Keith, M.A. Al-Laham, C.Y. Peng, A. Nanayakkara, M. Challacombe, P.M.W. Gill, B. Johnson, W. Chen, M.W. Wong, C. Gonzalez, and J.A. Pople, Gaussian, Inc., Wallingford CT, 2004.
[27] Gaussian 09, Revision A.02, M.J. Frisch, G.W. Trucks, H.B. Schlegel, G.E. Scuseria, M.A. Robb, J.R. Cheeseman, G. Scalmani, V. Barone, B. Mennucci, G.A. Petersson, H. Nakatsuji, M. Caricato, X. Li, H.P. Hratchian, A.F. Izmaylov, J. Bloino, G. Zheng, J.L. Sonnenberg, M. Hada, M. Ehara, K. Toyota, R. Fukuda, J. Hasegawa, M. Ishida, T. Nakajima, Y. Honda, O. Kitao, H. Nakai, T. Vreven, J.A. Montgomery, Jr., J.E. Peralta, F. Ogliaro, M. Bearpark, J.J. Heyd, E. Brothers, K.N. Kudin, V.N. Staroverov, R. Kobayashi, J. Normand, K. Raghavachari, A. Rendell, J.C. Burant, S.S. Iyengar, J. Tomasi, M. Cossi, N. Rega, J.M. Millam, M. Klene, J.E. Knox, J.B. Cross, V. Bakken, C. Adamo, J. Jaramillo, R. Gomperts, R.E. Stratmann, O. Yazyev, A.J. Austin, R. Cammi, C. Pomelli, J.W. Ochterski, R.L. Martin, K. Morokuma, V.G. Zakrzewski, G.A. Voth, P. Salvador, J.J. Dannenberg, S. Dapprich, A.D. Daniels, Ö. Farkas, J.B. Foresman, J.V. Ortiz, J. Cioslowski, and D.J. Fox, Gaussian, Inc., Wallingford CT, 2009.
[28] F. Terenziani, C. Katan, E. Badaeva, S. Tretiak, and M. Blanchard-Desce, Advanced Materials **20**, 4641 (2008).

[29] S. Tretiak and V. Chernyak, J. Chem. Phys. **119**, 8809 (2003).
[30] See supplementary material at http://dx.doi.org/10.1063/1.4939568 for the detailed information for theoretical calculation.
[31] L. Ji, R.M. Edkins, L.J. Sewell, A. Beeby, A.S. Batsanov, K. Fucke, M. Drafz, J.A.K. Howard, O. Moutounet, F. Ibersiene, A. Boucekkine, E. Furet, Z. Liu, J.-F. Halet, C. Katan, and T.B. Marder, Chem. Eur. J. **2014**(20), 13618–13635.
[32] D. Jacquemin and C. Adamo, *Computational Molecular Electronic Spectroscopy with TD-DFT*, Topics in Current Chemistry (Springer Berlin Heidelberg, 2015), pp. 1-29.
[33] C. Katan, P. Savel, B. M. Wong, T. Roisnel, V. Dorcet, J.-L. Fillaut, and D. Jacquemin, Phys. Chem. Chem. Phys. **16**, 9064–9073 (2014).
[34] W. Liang, H. Ma, H. Zang, and C. Ye, Int. J. Quantum Chem. **115**, 550–563 (2015).
[35] J. Cascante-Vindas, A. Díez, J. L. Cruz, and M.V. Andrés, Opt. Express **18**, 14535 (2010).
[36] S. Boinapally, B. Huang, M. Abe, C. Katan, J. Noguchi, S. Watanabe, H. Kasai, B. Xue, and T. Kobayashi, J. Org. Chem. **79**, 7822 (2014).